Three-phase AC-DC Converter for EV Rapid Charging with Wireless Communication for Decentralized Controller

Keita Ohata[1], Masakazu Adachi[1], Keisuke Kusaka[1] and Jun-ichi Itoh[1]

[1] Nagaoka University of Technology, Japan

Abstract-- **This paper proposes a multi-modular AC-DC converter system using wireless communication for a rapid charger of electric vehicles (EVs). The multi-modular topology, which consists of multiple modules, has an advantage on the expandability regarding voltage and power. In the proposed system, the input current and output voltage are controlled by each decentralized controller, which wirelessly communicates to the main controller, on each module. Thus, high-speed communication between the main and modules is not required. As the results in a reduced number of signal lines. The fundamental effectiveness of the proposed system is verified with a 3-kW prototype. In the experimented results, the input current imbalance rate is reduced from 49.4% to 0.1%, where total harmonic distortion is less than 3%.**

***Index Terms*- - AC-DC converter, decentralized controller, wireless communication, droop control**

I. Introduction

The multi-modular topology, which consists of multiple modules, has an advantage on the expandability regarding voltage and power [1-12]. Thus, the multi-modular topology is suitable for high-voltage, and high-power converters. Considering a rated voltage of IGBTs or SiC MOSFETs, the several dozen modules is required for 6.6-kV input.

However, an increase in the number of modules causes complexity of wired communication between the main controller and each module because a current and voltage information for feedback control, thermal information for safety, gate signals must be transmitted to the main controller. In addition, the communication of the input current information must be fast because the centralized controller directly control the input current [13-18]. Generally, a band width for the input current control must be higher than several thousand radian per seconds considering the grid frequency. Thus, the communication must be wired communication .

In this paper, the control method with wireless communication by the droop control and the current balancing control using wireless communication between the main controller and the controller with wireless communication on each module is proposed. In the proposed control, the input current and the output voltage are independently controlled by each module. Owing to the droop control and the current balancing control, low-speed communication between the main and module controller can be accepted because the input current and output voltage is independently controller by each controller on the modules.

This paper is organized as follows. In section II, the wireless modules on the market is tested because a limitation of the frequency band of the wireless communication must be clear. Next, the proposed control with wireless communication by the droop control and the current balance control which used wireless communication module are explained in section III. Then the proposed method is confirmed by the experiments.

II. Evaluation of Wireless Communication System

In this chapter, a Bluetooth module for the wireless communication of the DC voltage command, which is used for the proposed control for an AC-DC converter, is evaluated. The DC voltage command is transmitted via the Bluetooth modules. In this evaluation, the limitation of the frequency band of the DC voltage control is experimentally tested. Note that, a buck chopper is used for the evaluation for simplicity.

A. Experimental condition

Table I lists the specification of the wireless module used in this test. The module of Bluetooth 4.1 is used in order to save power consumption. Besides, microchip low-energy data profile is used as a Bluetooth profile. The profile performs as communication of UART (universal asynchronous receiver transmitter).

Table II lists the specification of the controller in the experiment for evaluation of a wireless communication system.

Figure 1 shows the outline of the test environment for the wireless communication with a buck chopper. The output voltage command is wirelessly transmitted. The controller on the buck chopper controls the output voltage according to the output command. In this experiment, the output voltage command value V_o* is sinusoidal with an amplitude of 30 V, and a DC bias of 100 V. The microprocessor #1 converts analog to digital in order to generate the command value. The analog command value is sampled with a sampling frequency of command value $f_{samp\text{-}c}$. The converted digital command value is sent to the microprocessor #2 via the Bluetooth modules #1. In the microprocessor #2, the inductor current control and the output voltage control are performed in order to follow the output voltage command value V_o^* and drive the step-down chopper. Besides, current control and voltage control are performed by microprocessor #2. Fig. 2 shows a circuit configuration of the buck chopper.

TABLE I. SPECIFICATION OF WIRELESS MODULE.

Manufacture	Microchip
Communication standard	Bluetooth ver. 4.1
Product name	RN4020
Module size	13.4 mm × 25.8 mm × 2 mm
Maximum speed	240 kbps
Allowable transmission distance	20 m

TABLE II. SPECIFICATION OF CONTROLLER AND MAIN CIRCUIT IN EXPERIMENT FOR EVALUATION OF WIRELESS COMMUNICATION SYSTEM

Quantity	Symbol	Value
Rated output power	P_n	1.0 kW
Range of output voltage	V_o	$283(200\sqrt{2}) \sim 150$ V
Rated output current	$I_{n\,(output)}$	6.67 A (@150 V)
Back-boost reactor	L	2.93 mH
Input capacitor	C_i	650 μF
Output capacitor	C_o	650 μF
Switching frequency	f_{sw}	10 kHz
ACR cutoff frequency	f_{ACR}	23.9 Hz
AVR cutoff frequency	f_{AVR}	239 Hz
Sampling frequency of command value	$f_{samp\text{-}c}$	10 kHz

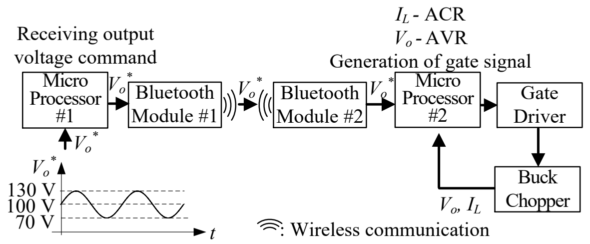

Fig.1 Outline of the buck chopper control system. The output voltage V_o is wirelessly provided.

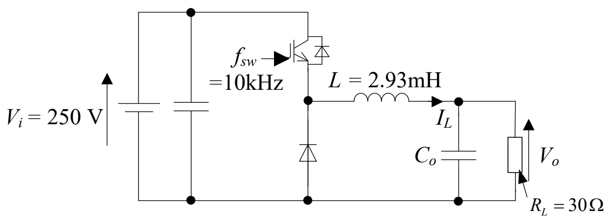

Fig. 2. Circuit configuration of the buck chopper

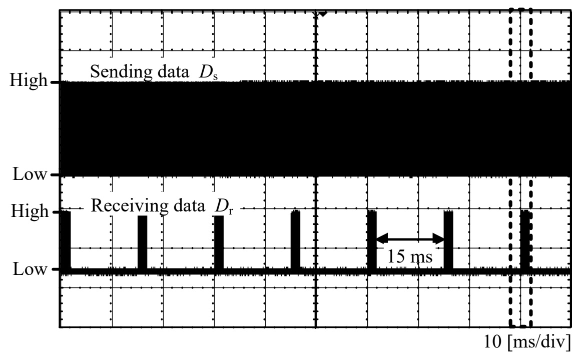

(a) Outline.

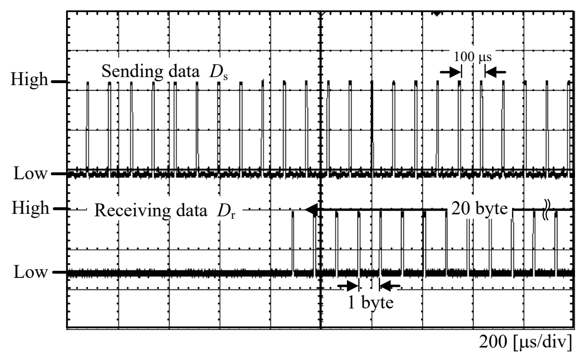

(b) Enlarge of Fig. 4. (a).

Fig. 3. Waveforms of sending data and receiving data. Fig. 7 (a) shows a waveform capturing sending and receiving data for a long time. As a result, even if data is continuously input to the module, it is actually sended intermittently and it can be seen that there is an interval of 15 ms. Fig. 7 (b) is an enlargement of (a).

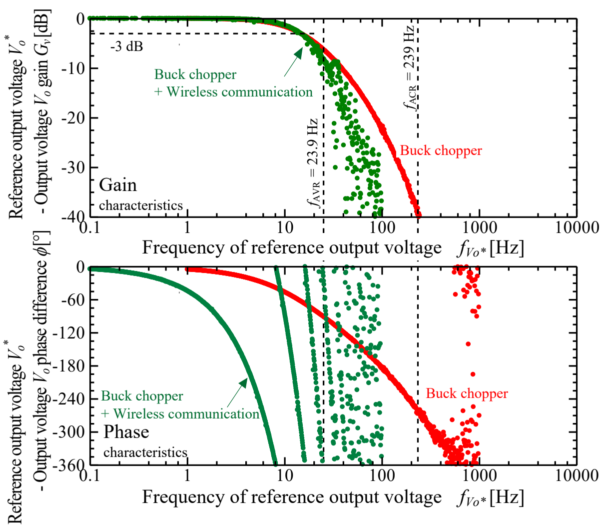

Fig. 4. Frequency characteristic of the output voltage V_o on the buck chopper.

B. Signal transmission

Figure 3 shows the send data of the Bluetooth module and the received data by another Bluetooth module. Note that the transmission data configuration has no parity and the transmission speed is 115.2 kbps. The data is constant at $(FF)_{16}$, and data is transmitted every 100 μs. From the above transmission data condition, the signal becomes high-level only when it represents the stop bit. Therefore, the number of bytes can be counted by counting the number of pulses that becomes High-level. Figure 3 (a) shows waveforms of send and received data. As a result, processing of the header and footer data which are added at the time of wireless communication causes about 15 ms of waiting time every 20 bytes. Figure 3(b) shows an enlargement of (a). In the figure, the sending and received data at once are 20 bytes. From the results, it is clear that the throughput is 11 kbit/s when the selected module is used.

C. Frequency characteristics with wireless communication

Figure 4 shows the frequency characteristic of output voltage V_o for the control system, which is obtained with varying the frequency of the output voltage command within 0.1 Hz to 10 kHz. The red dots are the response of the buck chopper without a wireless communication, and the green dots are the response of step-down chopper with the output voltage command provided by wireless communication. Figure 4 (a) shows the gain characteristics. Regardless of whether wireless communication is used, the gain decreases monotonously from around 10 Hz. After that, the gain continuously decreases in the buck chopper without wireless communication. On the other hand, in the buck chopper given by wireless communication, the gain decreases with a variability due to the transmission time. Fig. 4 (b) shows the phase characteristics. The change rate of the phase difference rapidly decreases from around 1 Hz, and the phase difference crosses 180 degrees at 4 Hz. Then, the phase difference monotonically decreases, especially the phase delay reaches 360 degrees at 9 Hz. As the results, the maximum frequency band of the output voltage command of the AC-DC converter should be less than 1 Hz.

As the result, it has been confirmed that wireless communication cannot be applied to the control requiring a wide frequency bands. Thus a new control method, which does not need wide frequency band communication, is required to employing the wireless communication.

III. Proposed Multi-Modular Converter System

A. Circuit Topology

Figure 5 shows the multi-modular AC-DC converter for the EV rapid charging. Each phase consists of multiple modules. The modules are connected in series on the primary side and connected in parallel on the secondary side. Each module has a PFC stage and isolation stage by the series-resonant DC-DC converter. The proposed system has the main controller, which transmits the output voltage reference using wireless communication, and controllers on each module. Each module independently controls the input current for PFC and output voltage without wired communication. The resonant DC-DC converter is operated in an open-loop.

The duty of the DC-DC converter is controlled as 50% used open-loop.

B. Decentralized Control with Wireless Communication

Figure 6 shows the proposed control block diagram. The main controller and module controllers operate the AC-DC converter. Each module controller assumes the output DC voltage control and the input current control as a minor loop of the output voltage control.

The output voltage V_o, input current I_u, I_v, and I_w are controlled by each phase module. Thus, high-performance controller is not necessary as the main controller because the output voltage is DC.

The input current commands i_{Lu}*, i_{Lv}*, i_{Lw}* are calculated from the amplitude of the current I_{amp} and the phase information θ_u, θ_v, θ_w as shown in (1).

$$\begin{aligned} i_{Lu}^* &= I_{amp}\left|\sin\theta_u\right| \\ i_{Lv}^* &= I_{amp}\left|\sin\theta_v\right| \\ i_{Lw}^* &= I_{amp}\left|\sin\theta_w\right| \end{aligned} \tag{1}$$

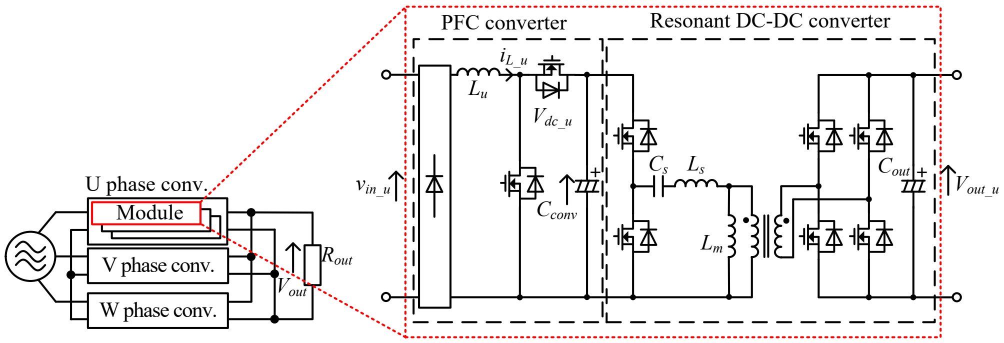

Fig. 5. Multi-modular AC-DC converter for EV Rapid Charging.

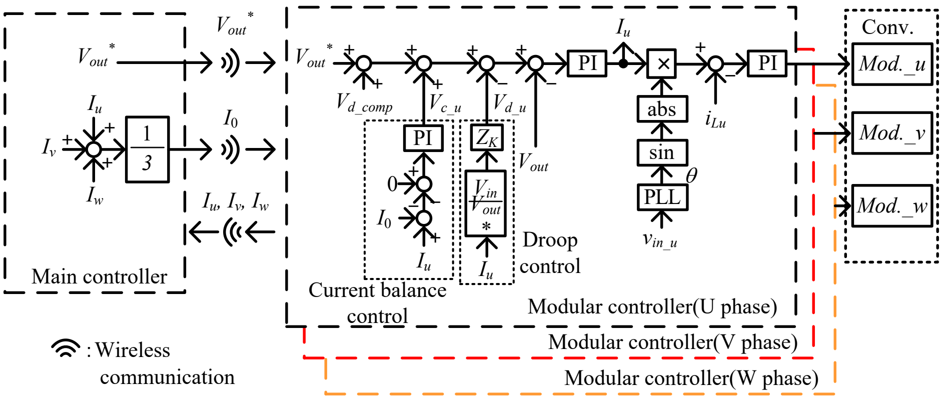

Fig. 6. Proposed decentralized control with wireless communication.

Note that θ_u, θ_v, θ_w are introduced using the PLL, and the phase current i_{Lu}, i_{Lv}, i_{Lw} in the inductors L_u, L_v, L_w are controlled as the absolute value of sine wave. It is characterized that the common output DC voltage is independently controlled by the module controllers to follow the output voltage command, which is wirelessly transmitted from the main controller.

The main controller is only used for generating the output DC voltage reference V_o^* and calculate the average current reference I_o. Two commands date are wirelessly sent to each phase module.

B.1. Droop control

In the proposed control scheme, the common output DC voltage is controlled by the multiple controllers. When the output voltage detection has an error in this configuration, it results in current unbalance between the phases and an increase in power loss. Thus, the droop control is employed in order to avoid the divergence from the output voltage even when a detection gain of the output voltage has an error.

Figure 7 shows the equivalent circuit of the output DC side with or without the droop control. The voltage $V_{\text{out\_u}}$, $V_{\text{out\_v}}$, and $V_{\text{out\_w}}$ are the output voltages of respective cells, and V_{out} is an output voltage applied to a load. Each module has an automatic voltage regulator to obtain the constant output voltage, the output voltage of each module can be represented as the ideal DC source as shown in Fig. 7. However, the temperature drift or settling error may occur detection value error. When the detected value has an error, one or two modules connected in parallel on the secondary side may stop the operation owing to a circulating current among modules.

Therefore, in the droop control, virtual resistance in series with the voltage source of each phase is introduced. The droop control is operated by dropping the dc voltage command value according to the droop gain K in order to make the voltage gain within the range of the droop gain K. The divergence of the output voltage control is suppressed by settling the droop gain K higher than a predicted detection error.

Droop control is applied to the voltage command value of the AVR. The droop voltages $V_{\text{d\_u}}$, $V_{\text{d\_v}}$ and $V_{\text{d\_w}}$ which are output by the droop control are expressed by the respective phase currents and the virtual resistance Z_K by the following (2).

$$\begin{aligned} V_{d\_u} &= \frac{V_{in}}{V_{out}*} Z_K \times I_u \\ V_{d\_v} &= \frac{V_{in}}{V_{out}*} Z_K \times I_v \\ V_{d\_w} &= \frac{V_{in}}{V_{out}*} Z_K \times I_w \end{aligned} \tag{2}$$

where The virtual resistance Z_K is determined by multiplying the droop gain $K_{\text{p.u.}}$.

The droop voltage is multiplied by the equivalent resistance gain in consideration of the voltage ratio on the primary side and the secondary side. On the other hand, the

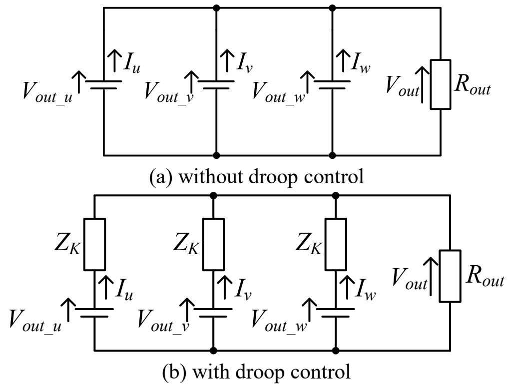

Fig. 7. Equivalent circuit of the output DC side with or without the droop control.

current flowing through the virtual resistor Z_K is expressed by (3).

$$\begin{aligned} I_u &= \frac{1}{Z_K}\left[V_{out\_u} - \left\{ \frac{R_{out}\left(V_{out\_u}+V_{out\_v}+V_{out\_w}\right)}{3R_{out}+Z_K} \right\} \right] = \frac{1}{Z_K}\left(V_{out\_u}-V_{out}\right) \\ I_v &= \frac{1}{Z_K}\left[V_{out\_v} - \left\{ \frac{R_{out}\left(V_{out\_u}+V_{out\_v}+V_{out\_w}\right)}{3R_{out}+Z_K} \right\} \right] = \frac{1}{Z_K}\left(V_{out\_v}-V_{out}\right) \\ I_w &= \frac{1}{Z_K}\left[V_{out\_w} - \left\{ \frac{R_{out}\left(V_{out\_u}+V_{out\_v}+V_{out\_w}\right)}{3R_{out}+Z_K} \right\} \right] = \frac{1}{Z_K}\left(V_{out\_w}-V_{out}\right) \end{aligned} \tag{3}$$

where V_{out} is output DC voltage, and V_{out_u} is an output voltage of each phase including an error. According to (3), the output current of each cell is determined by the difference of the potential between V_{out_x} and V_{out} and the virtual resistance. At this time, (4) must be satisfied.

$$\begin{aligned} V_{out\_u} &> V_{out} \\ V_{out\_v} &> V_{out} \\ V_{out\_w} &> V_{out} \end{aligned} \tag{4}$$

If the V_{out_u}, V_{out_v}, V_{out_w} are less than V_{out}, the output current will be negative. Therefore, the current flows from the output side to input side; then, the PFC will stop the operation. Note that, each phase currents should be positive to let PFC work in each module. V_{out} is given from (3) as (5)

$$V_{out} = \frac{V_{out\_u}+V_{out\_v}+V_{out\_w}}{3+K_{p.u.}} \tag{5}$$

Next, the case where the voltage detector contains a detection error is considered to determine the droop gain. Assuming that the U phase includes detection error, the error is defined as Err_u[p.u.]. From equation (5), the output DC voltage including the detection error is given by (6).

$$V_{out} = \frac{V_{out\_u}(1+Err\_u)+V_{out\_v}+V_{out\_w}}{3+K_{p.u.}} \quad (6)$$

Therefore, minimum droop gain $K_{p.u}$ is given by (7).

$$Err\_u < K_{p.u.} \quad (7)$$

In addition, output DC voltage V_o is decreased by droop gain $K_{p.u}$. In this time, voltage controller compensates the decreased V_o using feed-forward control. As understood from (5), imbalanced input current occur only with the droop control. Therefore, current balance control is applied.

B.2. Current balancing control

The droop control avoids the output voltage from the divergence. However, the droop control does not balance the input current. Thus, the current balancing control is employed.

In this control, phase currents are averaged using (8) by main controller. Secondary, the main controller calculates the averaged output DC current command value I_o^*. DC current command values I_u*, I_v*, I_w* of each phase in the module controller generate the deviation, which is compensated by the voltage controller. In this control, firstly, phase currents are averaged using (8) by the main controller.

$$I_0^* = \frac{I_u^* + I_v^* + I_w^*}{3} \quad (8)$$

Secondly, the averaged output DC current command value I_0* and DC current command values I_u^*, I_v^*, I_w^* of each phase are calculated. In addition, the deviation between I_0^* and I_u^*, I_v^*, I_w^* is calculated. Thirdly, the module controller adjusts the deviation to zero using feed-forward control.

IV. Experimental Results

This chapter describes that the result of the experimental results with a 3-kW prototype. Table III lists the experimental conditions.

A. Steady state response

Figure 8 shows the comparison between the input current without or the droop and balance control. In order to emulate the voltage detection error, the output voltage detection value on u-phase is decreased by 10% on purpose. The input current is not sinusoidal and it is unbalanced when the droop and balance control are not employed as shown in Fig. 8 (a). By contrast, the input current is sinusoidal when the proposed control is employed as shown in Fig. 8 (b).

Figure 9 shows the operating waveforms of the input voltage, input current, and the output voltage. The input

TABLE III. EXPERIMENTAL CONDITIONS.

Quantity	Symbol	Value
Input voltage	v_{in}	200 V
Rated power	P	3 kW
Conveter capcitance	C_{conv}	48 µF
Output capcitance	C_{out}	680 µF
Input inductance	L	3 mH
Load resistance	R_{out}	40 Ω
Voltage reference	V_{dc}*	350 V
Switching frequency (PFC)	f_{sw}	20 kHz
Resonant frequency (Resonant DC-DC converter)	f_o	50 kHz
Angular frequency of ACR	ω_{ACR}	6000 rad/s
Angular frequency of AVR	ω_{AVR}	50 rad/s
Proposal gain of current balance control	$K_{\_c}$	2.0

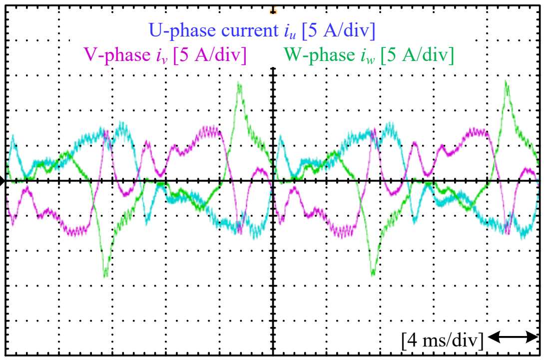

(a) Without proposed control.

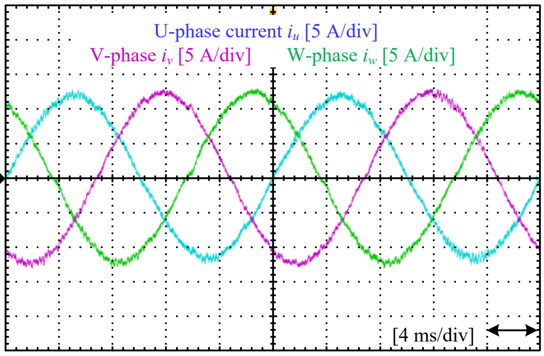

(b) With proposed control.

Fig. 8. Comparison of input current. The input current is balanced using the droop control and the current balance control.

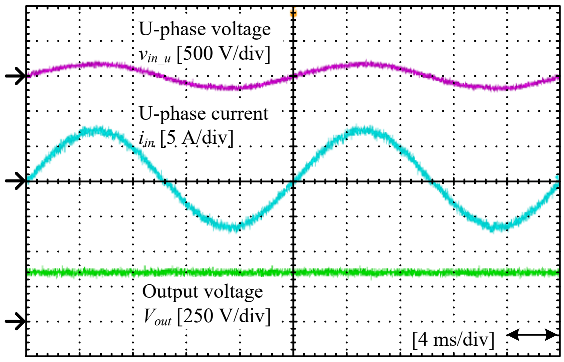

Fig. 9. Operating waveforms of input voltage, input current and output voltage.

current is sinusoidal and output voltage ripple is slight from Fig. 8. In this condition, input current THD is 3%. Imbalance rate of the input current is 1%. Note that the imbalance rate of input current defined by

$$\varepsilon_{current\_err}[\%] = \left| \max\left\{ \frac{I_u - I_{avg}}{I_{avg}}, \frac{I_v - I_{avg}}{I_{avg}}, \frac{I_w - I_{avg}}{I_{avg}} \right\} \times 100 \right| \quad (9)$$

where I_{avg} is the average of phase currents. The output voltage is following to the reference value with an uncertainty of 1%. In addition, output voltage ripple is slight. Ripple rate of the output voltage is 0.3%. Note that this rate defined by the following

$$\varepsilon_{voltage\_ripple}[\%] = \left| \frac{V_{o(p-p)}}{V_{o(avg)}} \times 100 \right| \quad (10)$$

B. Effect of communication delay

B.1. imbalanced input current

The average command value of input current may fluctuate when communication delay is imbalanced between the main controller and phase module. In order to simplify the communication among them, U-phase current signal is assumed to have a communication delay. The command value of the output current with the effect of communication delay is given by

$$I_0^* = \frac{(I_u^* \times D_{\_err}) + I_v^* + I_w^*}{3} \quad (11)$$

where D_{err} is U-phase signal error rate by communication delay. The balance control of the phase currents uses the command value of the average of output DC current I_0 and command value of each modules. The feed-forward voltage is given by

$$\begin{aligned} V_{c\_u} &= (I_0 - I_u) \times K_{\_c} \\ V_{c\_v} &= (I_0 - I_v) \times K_{\_c} \\ V_{c\_w} &= (I_0 - I_w) \times K_{\_c} \end{aligned} \quad (12)$$

where K_c is the proportional gain of the current balance controller.

In this case, V_{c_u}, V_{c_v}, V_{c_w} is proportional to the K_c. Thus, output voltage is changed by the error which is included in the command value of current. Therefore, the allowable range of error rate of phase current should be revealed in the real system. As an example, consider command value of phase current using the specifications of CHAdeMO standard. The standard is allowed output voltage error ±5%. Thus, if output voltage is decided as 350 V, the converter must be controlled between 332.5V to 367.5V.

Figure 10 shows the output voltage when U-phase current signal is assumed to have the communication delay. Fig. 10 confirms that the range of the current signal error rate satisfies the CHAdeMO standard. From this figure, the current signal value error allow about ±30%.

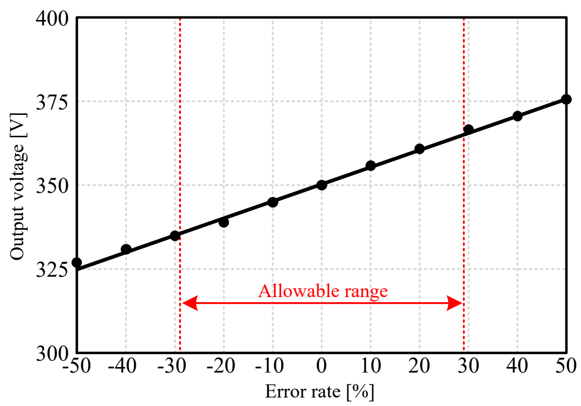

Fig. 10. Output voltage when U-phase current signal is assumed to have communication delay.

C. Effect of calculation cycle

Figure 11 shows the variation rate of output voltage when calculation cycle is changed from 100 ms to 1s. This experimental condition is listed in Table III. Output voltage variation rate is increased by the increase of the operation cycle. On the other hand, it was confirmed that the voltage fluctuation rate falls within 5% if one operation cycle requires less than the one second. Therefore it was confirmed that the main controller does not require high performance.

D. Step response

Figure 12 shows step response waveform of phase current. In this case, output power changes 1 kW to 2 kW. The current was not largely unbalanced when the step reference of output voltage. The current waveform is slightly unbalanced because the update timing of the current command value I_o differs among the modules due to the communication delay.

V. Conclusion

This paper proposes the decentralized control with wireless communication of multi-modular AC-DC converter for EV rapid charging. First, Bluetooth (Ver. 4.1) was taken as an example of wireless communication, and the requirements for introducing wireless communication into control were confirmed. Moreover, the configuration of the assumed three-phase AC-DC converter and the droop and balance control method are described. It is demonstrated that the proposed control achieves the input current balancing and the output voltage control without wired communication between the main controller and phase module. As the experimental results, the imbalance rate of the input current was 1% or less, and the input current THD was 3% or less. In addition, the output voltage follows the voltage command value at 1% or less, and the output voltage ripple rate achieves 0.3% or less.

It was also confirmed that the output voltage error is within ± 5% (350 ± 17.5V). It will satisfyming to the CHAdeMO standard if there is an detection error of ±30% or less in the command value of input current when the output voltage command value is 350V. In addition, we confirmed that even if there was a communication delay of 1 s, the input current balance was well controlled without breaking. This control with wireless communication is expected to be a versatile technology applicable to the control of any multi-modular converter as well as the three-phase AC-DC converter, and its future application is expected.

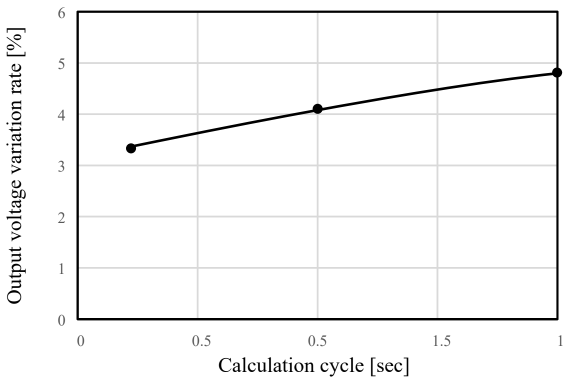

Fig. 11. Variation rate of output voltage when calculation cycle is changed.

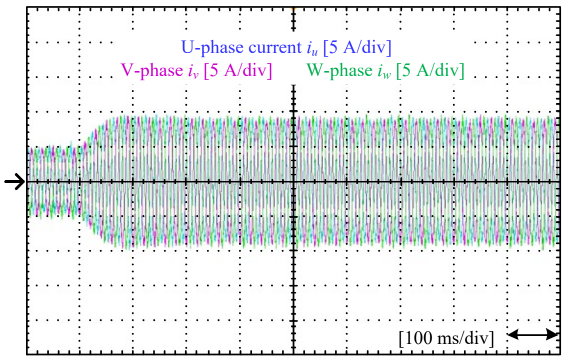

(a) Outline.

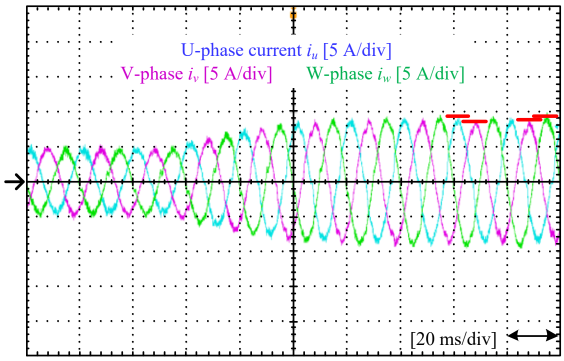

(b) Enlarge of Fig. 11. (a).

Fig. 12. Step response waveform of phase current.

REFERENCES

[1] V. Chunkag, Uthen Kamnarn, “Nearly Unity Power-Factor of the Modular Three-Phase AC to DC Covnerter with Minimized DC Bus Capacitor,” *IEE of Japan Transactions on Industry Applications*, vol. 128, No. 8, pp. 979-988, 2008

[2] X. Yu, X, She, X. Zhou and A. Q. Huang: “Power Management for DC Microgrid Enabled by Solid-State Transformer”, *IEEE Trans.*, Vol.5, No.2, pp.954-965 2014

[3] T. Zhao, G. Wang, S. Bhattacharya, and A. Q. Huang: “ Voltage and Power Balance Control for a Cascaded H-Bridge Converter-Based Solid-State Transformer”, *IEEE Trans.* On Power Electronics, Vol. 28, No. 4, pp.1523-1532, 2013

[4] A. A. Milani, M. T. A. Khan, A. Chakrabortty and I. Husain, “Equilibrium Point Analysis and Power Sharing Methods for Distribution Systems Driven by Solid-State Transformers” *IEEE Transactions on Power Systems*, vol. 33, no. 2, pp. 1473-1483, 2018

[5] J. Ramos-Ruiz, H. Krishnamoorthy, and P. Enjeti: “Adding Capacity to an Existing Electric Power distribution Network using a Solid State Transformer system”, *ECCE 2015*, pp.6059-6066 2015

[6] J. E. Huber, and J. W. Kolar: “Solid-State Transformer: On the Origins and Evolution of Key Concepts”, *IEEE Industrial Electronics Magazine*, Vol. 10, pp.19-28 2016

[7] Dennis Karwatzki, Axel Mertens: “ Generalized Control Approach for a Class of Modular Multilevel Converter Topologies”, IEEE Transactions on Power Electronics, Vol. 33, pp.2888 – 2900, 2018

[8] M. Nakahara, and K. Wada, “Loss Analysis of Magnetic Components for a Solid-State-Transformer,” *IEE of Japan Journal of Industry Applications*, Vol.4, No.7, pp.387-394, 2015

[9] Yusuke Hayashi, Tamotsu Ninomiya, “Highly Scalable Sensorless Multicellular AC-DC Transformer (ADX) for the DC Distribution System in Data Centers”, *IEE of Japan Journal of Industry Applications*, vol. 7, No. 6, pp. 479-487, 2018

[10] Yusuke Hayashi, Yoshikatsu Matsugaki, and Tamotsu Ninomiya “Capacitively Isolated Multicell Dc-Dc Transformer for Future Dc Distribution System," *IEE of Japan Journal of Industry Applications*, vol. 6, no. 4, pp. 268-277, 2017

[11] Toshiki Nakanishi, and Jun-ichi Itoh, “Design Guidelines of Circuit Parameters for Modular Multilevel Converter with H-bridge Cell”, *IEE of Japan Journal of Industry Applications,* vol.6, no.3, pp.231-244, 2017

[12] Toshiki Nakanishi, and Jun-ichi Itoh,"Control Strategy for Modular Multilevel Converter based on Single-phase Power Factor Correction Converter", *IEE of Japan Journal of Industry Applications,* vol.6, no.1, pp.46-57, 2017.

[13] X. Wang, J. Liu, S. Ouyang, T. Xu, F. Meng, S. Song: “Control and Experiment of an H-Bridge-Based Three-Phase Three-Stage Modular Power Electronic Transformer”, IEEE Transactions on Power Electronics, Volume: 31, Issue: 3, pp.2202-2011 2016

[14] N. F. Avila, C. Chu: “Distributed Pinning Droop Control in Isolated AC Microgrids”, *IEEE Transactions on Industry Applications,* Volume: 53, Issue: 4, pp.3237-3249, 2017

[15] X. Chen, L. Wang, H. Sun, Y. Chen: “Fuzzy Logic Based Adaptive Droop Control in Multiterminal HVDC for Wind Power Integration”, IEEE Transactions on Energy Conversion, Volume: 32, Issue: 3, pp.1200-1208, 2017

[16] G. Li, Z. Du, C. Shen, Z. Yuan, G. Wu “Coordinated Design of Droop Control in MTDC Grid Based on Model Predictive Control”, IEEE Transactions on Power Systems, Volume: 33, Issue: 3, pp.2816-2828, 2017

[17] B. Berggren, K. Linden, R. Majumder“DC Grid Control Through the Pilot Voltage Droop Concept—Methodology for Establishing Droop Constants”, IEEE Transactions on Power Systems, Volume: 30, Issue: 5, pp.2312-2320, 2014

[18] S. Augustine, M. Mishra, “Adaptive Droop Control Strategy for Load Sharing and Circulating Current Minimization in Low-Voltage Standalone DC Microgrid”, IEEE Transactions on Sustainable Energy, Volume: 6, Issue: 1, pp.132-141, 2014